Applied Catalysis B: Environmental 242 (2019) 397–409

Contents lists available at ScienceDirect

Applied Catalysis B: Environmental

journal homepage: www.elsevier.com/locate/apcatb

Optimised cycling stability of sorption enhanced chemical looping steam reforming of acetic acid in a packed bed reactor

Oluwafemi A. Omoniyi*, Valerie Dupont

School of Chemical and Process Engineering, University of Leeds, LS2 9JT, UK

ARTICLE INFO

Keywords:
Sorption enhancement
Chemical looping
Steam reforming
Acetic acid
Nickel
Hydrogen production
Sorbent hydration

ABSTRACT

The cycling stability of reactor bed materials during the production of enhanced high purity hydrogen in the sorption enhanced chemical looping steam reforming (SE-CLSR) of acetic acid was studied and compared with the conventional steam reforming process. A packed bed reactor was used at 1 atm with a nickel catalyst supported on calcium aluminate intimately mixed with CaO in the role of high temperature CO_2 sorbent. Twenty cycles of SE-CLSR were conducted under combined NiO-reduction/HAc steam reforming at 650 °C, at feed molar steam to carbon ratio of 3 and WHSV of 1.18 h^{-1}, cyclically alternating with air feed to perform the coupled Ni-oxidation and $CaCO_3$ calcination at 850 °C. Sustained and consistent reforming was achieved in excess of 80% of HAc conversion across all 20 SE-CLSR cycles; this was accompanied by hydrogen yield efficiencies exceeding 78% when compared to equilibrium values at same conditions. However, by the end of the 20th cycle, the extent of CaO carbonation had dropped to about 50% of that observed in the first cycle. Five SE-CLSR cycles were run using steam hydration at 250 °C prior to the fuel feed with the aim of improving sorbent conversion. A higher hydrogen yield was observed with an increase in fuel conversion. The sorbent conversion was also stable across all 5 SE-CLSR cycles when performed with sorbent pre-hydration using steam. This was attributed to an increased carbonation rate during the sorbent's pre-breakthrough period. Enhanced auto-reduction of the NiO catalyst resulting from sorption of the CO_2 product was also observed, and an improved sorbent conversion outlook over the cycles was investigated. TEM and SEM images indicated that carbon formed during the fuel-feed stage was eliminated during the cyclic oxidation step.

1. Introduction

The global need for hydrogen is poised to grow significantly due to its increasing demand as a valuable raw material in many chemical and petroleum industries, in addition to its potential utilisation as a clean fuel and energy vector. It is also driven by the breadth of sources and processes by which it can be produced such as electrolysis, photo-electrolysis as well as via catalytic reforming of fossil fuels and renewable sources [1]. There is however increased research in the production of hydrogen from renewable resources notably biomass due to the large environmental impacts realised from its production from fossil fuels. Biomass resources have the potential to be sustainable feedstocks for hydrogen production; however there are challenges in relations to cost and conversion efficiencies, perception and the knowledge of economically viable options [2,3]. The production of hydrogen from biomass can be achieved through biological processes

Abbreviations: HAc, Acetic acid; C-SR and C-SMR, Conventional steam reforming, Conventional steam methane reforming; PSA, Pressure Swing Adsorption; CLSR, Chemical Looping Steam Reforming; SESR and SE-CLSR, Sorption Enhanced Steam Reforming, Sorption Enhanced Chemical Looping Steam Reforming; OC, Oxygen Carrier; TEM and SEM, Transmission electron microscope and Scanning electron microscope; CHN, Carbon, hydrogen and nitrogen elemental analysis; BET, Brunauer–Emmett–Teller method; ICP-MS, Inductively coupled plasma mass spectrometry; TOC, Total Organic Carbon; S/C, Steam to Carbon ratio; sccm, Standard cubic centimeters per minute; X_{HAc} and X_{H2O}, Conversion fraction of acetic acid and steam respectively; WHSV, weight hourly space velocity; T_{SR}, T_{OX} T_{HY}, Temperature of Steam reforming oxidation and hydration respectively; PB, BT SS, Pre-breakthroughbreakthrough andpost breakthrough steady state stages; $\dot{n}_{out,dry}$, Total molar flow rate dry basis; n_i, number of moles of specie I; y_i and y_a, molar fraction of specie i and all gases in the outlet gas respectively; Sel_i, Selectivity of individual constituent; W_i, Molar weight of specie I; $\dot{n}_{i,in}$ *and* $\dot{n}_{i,out}$, molar flow rate in and out of specie i respectively; $\dot{n}_{c,gas}$, n_{Cgas}, Molar rate, Number of moles of carbon gasified in air feed stage; T_{BT}, T_{SS} T_0, Time at breakthrough, onset of steady state and onset of pre breakthrough phase; $\check{n}_{NiO\rightarrow Ni,ss}$, Rate of NiO reduction to Ni; T_{FR}, time to full catalyst reduction; $\dot{n}_{CO_2,CARB}$, molar rate of CO_2 consumed by carbonation; X_{CO_2}, Eff_{PB}, conversion of CO_2, sorbent, efficiency of the sorbent conversion; R_{red}, reduction rate efficiency; SECAR, Sorption enhanced catalyst auto-reduction

* Corresponding author.
E-mail addresses: oluwafemi.omoniyi@outlook.com (O.A. Omoniyi), v.dupont@leeds.ac.uk (V. Dupont).

https://doi.org/10.1016/j.apcatb.2018.09.083
Received 16 August 2018; Received in revised form 17 September 2018; Accepted 25 September 2018
Available online 30 September 2018
0926-3373/

[4] or thermochemical means. The thermochemical process routes can be done either through gasification of biomass [5] or the catalytic steam reforming of biomass derived volatiles [6]; the latter particularly with the use of bio-oils or its model compounds have shown great promise [7–9]. Steam reforming of acetic acid as a model compound of bio-oils has been investigated in the past due to its presence in high concentrations in the water-soluble fraction of pyrolysis oil [10–12].

The steam reforming of pyrolysis oils and its model compounds generates a significant amount of CO_2 just like in conventional steam methane reforming (C-SMR), which prompts the need for extra hydrogen purification steps; these can be done primarily though Pressure Swing Adsorption (PSA) or other techniques (absorption, cryogenic separation), which increase either the energy requirements and or the capital costs associated with the production of high purity hydrogen. Another downside realised from the steam reforming of HAc, as is also the case for its parent bio-oil, is excessive coking and carbon deposition on the catalyst [13,14]. This leads to a reduction of the operating life of reforming catalysts, and lowers the overall efficiency of the steam reforming process due to shorter reforming times and the need for frequent off line catalyst regeneration [9,15]. This has prompted studies on intensification measures of reforming, such as chemical looping steam reforming 'CLSR', which incorporate cyclic catalyst regeneration steps as integral part of the heat management [16–20]. In addition, sorption enhanced steam reforming 'SESR' is promoted to improve the efficiency of the conventional reforming process through in-situ high temperature CO_2 sorption [21–26]. Combining CLSR with SE-SR into SE-CLSR [27,28] can achieve mutual benefits or synergies in intensifying the steam reforming process.

The SE-CLSR process involves in-situ high temperature CO_2 capture through the introduction of a solid CO_2 sorbent into the reforming catalyst bed, where the latter doubles up as oxygen carrier for chemical looping. This can occur in a single packed bed reactor operating with alternating feed flows, with on cycle consisting of a fuel and steam feed, followed by an air feed. CO_2 sorption during fuel and steam feed enhances water gas shift with a positive knock on effect on both the steam reforming reaction and the catalyst reduction via the unmixed combustion reaction (by higher consumption of CO and removal CO_2). During catalyst oxidation under air feed, both catalyst and sorbent undergo regeneration. Heat release and heat demand during fuel and steam feed can achieve coupling of endothermic reduction-reforming with exothermic CO_2 chemisorption resulting in high yield and purity hydrogen being produced near autothermally. This alternates with exothermic carbon and nickel oxidations being coupled with endothermic sorbent calcination, thus regenerating the bed materials under air feed, near autothermally too. Lack of temperature gradients during cycles of SE-CLSR should offer optimum conditions for an energy efficient process by avoiding generation of entropy. The need for separate water gas shift reactor, purification column, and external heating is either eliminated or greatly reduced compared to conventional steam reforming. The SE-CLSR of biomass derived liquids has been previously investigated [27–29]; it is generally agreed that it leads to an increase in the yield and purity of hydrogen produced due to the shift in equilibrium caused by the sorption activity [29,30]. A study on the SE-CLSR of ethanol indicates that the presence of the sorbent has positive impacts on the external heat demand and system requirements, it also indicates that the ratio of sorbent to catalyst plays an important role in the conventional steam reforming process with respect to feedstock conversion and hydrogen selectivity [31].

The major challenge encountered in the SE-CLSR process has been attributed to the cyclic ability and proficiency of regenerated materials particularly the sorbent [32]. Loss of sorbent activity has been reported in several literature on the SESR process; a loss of sorbent activity was observed over three cycles when glycerol was steam reformed with in-situ sorption enhancement [33], this was attributed to a loss of CO_2 capture capacity as observed in SESR of methane [34,35].

The major cause of the sorbent deterioration particularly in CaO based sorbent has been attributed to the inability of the sorbent to re-carbonate fully from cycle to cycle after calcining at a high temperature; this is largely due to ash fouling, mass loss, and reduced porosity, which might arise through accelerated sintering, thus preventing diffusion of CO_2 into the sorbent material due to the collapse of pore particles [36–41].

CaO based sorbent are promoted as suitable adsorbents for the SE-CLSR process due to their low cost, availability, widespread abundance, and their adequate adsorption capacities at high temperatures; hence, suggested techniques for improving their cyclic stability and efficiency is being investigated. These techniques include sorbent modification, steam hydration and obtaining CaO from precursors [42]. Doping of the sorbent might also help increase the sorbent's resistance to attrition and reduce the decay of its capacity that might arise through sintering [43]. The use of thermal pre-treatment and self-reactivation [44], the utilisation of nanostructured CaO based sorbent [45,46] and the use of synthetic sorbents are also being investigated to improve the cyclic stability of CaO based sorbents [32,47,48]. The increase in stability and capture capacity particularly in the case of nanostructured or modified CaO material however, might bring about the need for higher temperatures of calcinations which might lead to increased sintering of the catalyst [25].

Direct and indirect hydration of CaO based sorbents has been shown to improve effectively the cyclic stability of sorbents; the process of indirect hydration for reactivation of CaO sorbents has been investigated in several studies [49,50]; it has been shown to lead to an increase in the surface area of the sorbent but might also lead to cracking and the production of fragile materials [49]. Materic et al. [51] also proposed that the attrition rate and fragile materials observed as a result of steam hydration could be avoided through what they termed superheated dehydration, this is done by dehydrating the calcined sorbent in a CO_2 environment. More interest has however been directed towards direct hydration; this is because it has been observed to result in higher carrying capacity, higher carbonation efficiency with less attrition [52,53].

This study investigates the redox cyclic ability and efficiency of the SE-CLSR of acetic acid in a packed bed reactor; 20 experimental SE-CLSR cycles were performed using a nickel-based steam reforming catalyst doubling as oxygen carrier (OC) in the chemical looping process, intimately mixed with a CaO based sorbent to achieve sorption enhancement effects and in situ CO_2 capture. The process outputs with time on stream and upon redox cycling were analysed and compared with chemical equilibrium values and stoichiometric data to measure consistency across the cycles. An overall carbon balance of the entire process per cycle and over the 20 cycles was also done to evaluate the proficiency of the process. The overall sorbent conversion during the carbonation period was also compared across the cycles, and the catalysts were characterised to determine changes in morphology. The effect of steam hydration on sorption related effects, including the newly observed "*sorption enhanced reduction*" of NiO is also evaluated. Five experimental SE-CLSR cycles were performed with sorbent direct pre-hydration and the resulting process outputs were also compared against equilibrium and stoichiometric values with the aim of evaluating changes in the process efficiency.

2. Experimental approach and methods

2.1. Materials and reactor set up

Acetic acid (HAc) purchased from Sigma-Aldrich (≥99%) was utilised as steam reforming feedstock while distilled water was used for every experimental run as the source of steam. The catalyst in this study (crushed and sieved to 250–650 μm) has been applied previously for steam reforming and CLSR [6,54] and contains 15 wt% NiO on a calcium aluminate support, while a CaO based natural sorbent supplied as granular limestone (Longcal SP25SA-grannular size < 1.0 mm) by

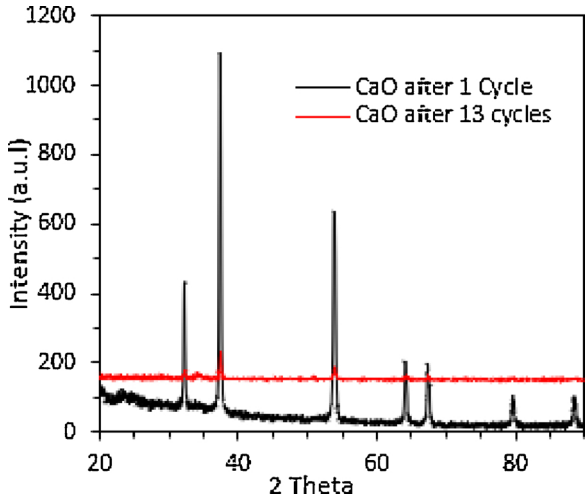

Fig. 1. XRD Pattern of calcined sorbent after one cycle and 13 cycles of calcination.

Longcliffe calcium carbonates was employed as sorbent material. The sorbent was activated by calcination before utilisation in the SE-CLSR experiments; this has been explored in many studies particularly with the view to stabilise the CO_2 carrying capacity of the sorbent [52,53].

Calcined sorbent was generated by subjecting the limestone to 13 cycles of carbonation and calcination in a packed bed reactor after an initial activation/calcination similar to those described in previous studies [53,55]. The activation and further calcination of the sorbent to generate activated sorbent was carried out at 850 °C in the presence of nitrogen while carbonation was carried out at 650 °C in the presence of pure CO_2, these has been reported to be ideal for calcination and carbonation of CaO based sorbents [53]. XRD patterns (Fig. 1) with Rietveld refinement indicate that the calcined sorbent utilised in the experimental runs contained 4.5% $CaCO_3$ and 95.5% CaO.

The reactor setup was a down flow system utilised in previous studies on steam reforming and CLSR of bio-derived liquids (condensates from fast pyrolysis of waste biomass) [6,54]. It consisted of a fully insulated packed bed reactor (1.27 cm internal diameter and 25 cm length) connected to aluminium and stainless-steel vaporisers. Fixed bed reactors can have advantages over fluidized bed specifically in Ni-based processes. This is because fluidized beds cause significant attrition with associated generation of fines which require constant purging and replacement. Thus, there is increased risk of Ni fines leakages to the surroundings, when Ni particulate matter is toxic when inhaled. For non-toxic bed materials, using fluidised beds which feature sorption processes proffer the advantage of easier regeneration by temperature swing due the use of dedicated reactors [56]. As fixed beds preserve the mechanical integrity of strongly supported Ni and are more suitable to large scales and high-pressure operation, they have been the preferred reactor type for steam methane reforming at industrial scale where Ni –based catalysis prevails (pre-reformer and primary reformer), typically only requiring replacing after three years of continuous operation. More details of the reactor set up can be found in Omoniyi and Dupont [54].

2 g of the activated/calcined crushed calcined sorbent were mixed with 2 g of the crushed NiO on calcium aluminate catalyst before introduction into the reactor for all SE-CLSR experiments. Extra experimental runs using 2 g of sand as inert diluting material in place of the sorbent were also conducted to assess the effect of the sorbent whilst maintain the same residence time in the reactor. Water and HAc were separately introduced into their vaporisers using gas tight 25 cm^3 syringes from SGE connected to two programmable syringe New Era Syringe Pumps systems. MKS mass flow controllers were utilised to regulate the flow of gases (H_2 for the first catalyst reduction, CO_2 for carbonation during sorbent pre-treatment, air during oxidation step of SE-CLSR, and N_2 during the HAc-steam feed to facilitate elemental balances). A Proportional Integral Derivative (PID) controller was utilised to regulate to set values the temperature of the reactor, that of the furnace and those of the two vaporisers. Gas product composition was measured by a two column Varian Micro-GC (CP 4900) after passing through a condenser and a further silica gel water trap. Galaxie software was used to observe the detected peaks and extract the data for further analysis. The first column of the micro-GC (molecular sieve 5 A) was operated with a backflush (13 s) and was used to detect H_2, O_2, CO, N_2, while the Pora plot Q collumn was used to monitor CO_2 and CH_4 as well as potentially C_2 and C_3 gases (although neither C_2 or C_3 gases were ever detected in the present experiments). Condensates were also collected from the condensate collector after every experimental run for elemental analysis to close the elemental balances over the cycles.

2.2. Experimental procedures

There are two basic stages in the SE-CLSR process of acetic acid; the HAc-steam feed stage and the air feed stage. The reactor system was purged with N_2 (200 sccm) at 650 °C before every experimental stage and run. Activation of the catalyst was done by reduction from its inactive oxide form to metallic Ni using 5% H_2/N_2 (244 sccm), this was carried out at 650 °C which was also the set temperature for the HAc –steam feed stage.

The overall reaction mechanism expected to occur in the HAc-steam-feed stage include the auto reduction of the catalyst, complete steam reforming, the carbonation of the sorbent and hydration reactions; T_{SR} was set at 650 °C as this is within the range observed for carbonation of CaO [53] and optimal sorption activity for the sorption enhanced steam reforming of acetic acid [24]. Previous studies also indicate that sustained steam reforming [8,15,21,57,58] and CLSR [54] of pyrolysis oils and its model compounds can be achieved at this T_{SR}. The acetic acid-steam feed stage was conducted at a feed molar steam to carbon ratio (S/C) of 3 and weight hourly space velocity (WHSV) of 1.18; the operating parameters utilised is within the range stated to be optimal for the SE-SR of acetic acid [22,23].

Three distinct time periods could be identified for all SE-CLSR fuel feed stage as described in previous studies [28]. The pre-breakthrough period (PB) features carbonation of the sorbent with negligible CO_2 present in the product gas; other carbonaceous products like CO and CH_4 are also expected to have negligible concentrations during PB as result of enhanced rate of carbonation and shifted equilibrium. The breakthrough period (BT) is triggered by the detection and increase of CO_2 from the process outputs as the sorbent approaches full capacity, the level of CO and CH_4 also tends to increase gradually in the product gas. When breakthrough concludes, manifested by CO_2 reaching its highest concentration, a new steady state is established (SS), the sorbent is fully saturated and constant level of CO_2 would be noticed at the product gas to indicate that sorption enhancement no longer occurs.

Steam hydration of the sorbent and catalyst material was carried out for ~30 min before each fuel feed stage using two values of T_{HY} (250 °C and 650 °C) in the presence of N_2 (50 sccm); it was expected that steam hydration used in pre-treatment of the sorbent would occur effectively at the lower temperature, whilst steam gasification of any remaining deposited carbon not burnt off during the previous oxidation period would be promoted at the higher temperature. The downside of the present approach is that steam hydration of sorbent is more effectively carried out under pressure, it is however assumed that partial hydration would occur efficiently at the lower temperature set and near atmospheric pressure of the reactor operation.

The periodic air feed stages were carried out at T_{OX} set to 800 °C–850 °C, this was done to ensure adequate calcination of the sorbent before re-use [53] whilst oxidising the Ni catalyst and gasifying additional deposited carbon as well. Air (200 sccm) was passed through the reactor until the concentration of oxygen detected in the micro-GC stabilised at ~21 Vol% with no CO_2 formation detected by the micro-GC.

2.3. Solids characterisation and analysis of condensates

The collected condensates recovered after every HAc-steam feed stage were analysed with the view to determine their carbon content and to evaluate possible leaching of catalyst. Possible leaching which has been identified in previous works on the steam reforming of model compounds of biomass derived oils [58] was evaluated through ICP-MS conducted using a SCIEX Elan 900 by Perkin Elmer. The carbon content in the condensates was calculated from TOC analysis using a Hach-Lange IL 550 analyser using the differential method; this would help in closing the overall carbon balance of the process per cycle, and with consecutive cycles.

Deposited carbon in the utilised bed material (sorbent and catalyst mix) was determined after the 20th HAc-steam feed stage using CHN elemental analysis. This was conducted in a flash EA 2000 elemental analyser. SEM and TEM imaging using a high-resolution Hitachi SU8230 and a FEI Tecnai TF20 respectively were also carried out to analyse surface topology, any changes in morphology, and the solid carbon product distribution. BET analysis was conducted using a Quantachrome Nova 2200e instrument to observe any changes in the open porosity and surface area of the used material.

2.4. Process outputs and material balances

$\dot{n}_{out,dry}$, the total molar dry gas flow rate was calculated from a nitrogen balance using the feed molar rate of N_2 and the molar fraction of N_2 detected by the micro GC ($\dot{n}_{out,dry} = \dot{n}_{N_{2,in}} / y_{N2}$.). this in turn was used to derive the HAc's carbon conversion to gases, X_{HAc} (Equation 1 A), from a carbon balance and subsequently, the steam conversion, X_{H_2O} (Equation 1B), from a hydrogen balance.

Equation 1 Conversion (fuel and steam)

$$X_{HAc}(\%) = 100 \times \frac{(\dot{n}_{out,dry} \times (y_{CO} + y_{CO_2} + y_{CH_4} + 2yC_2H_6 + 2yC_2H_4 + 3yC_3H_6 + 3yC_3H_8))}{2 \times n_{HAC,in}} \text{(A)}$$

$$X_{H_2O}(\%) = 100 \times \frac{(\dot{n}_{out,dry} \times (y_{H_2} + 2y_{CH_4} + 3y_{C_2H_6} + 2y_{C_2H_4} + 3y_{C_3H_6} + 4y_{C_3H_8}) - 2 \times n_{HAC,in} \times X_{HAc})}{n_{H_2O,in}} \text{(B)}$$

The sorption activity occurring in the PB and BT periods makes it difficult to calculate a meaningful value of X_{HAc} since the CO_2 intermediate product is immediately captured on the sorbent during PB and BT. It is generally agreed that the X_{HAc} would be higher in these phases when compared to that of the SS period because of the shift in equilibrium and higher carbonation rates caused by CO_2 sorption activity [21,28]. Hence, a minimum fuel conversion can be assumed for the PB and BT periods using the X_{HAc} calculated for the subsequent SS period.

$$X_{Hac,PB-min} = X_{Hac,BT-min} \approx X_{Hac,SS}$$

The hydrogen yield (wt. %) under HAc/steam feed is calculated using Equation 2 as a ratio of the mass flow rate of hydrogen in the process output to the mass flow rate of HAc feedstock (no water) The hydrogen purity on a dry basis (%) was also calculated as indicated in Equation 3;

Equation 2 Hydrogen yield (wt.%)

$$\text{Hydrogen yield (wt. \%)} = \frac{W_{H_2} \times 100 \times \dot{n}_{out,dry} \times y_{H_2}}{W_{HAC} \times n_{HAC,in}} = \frac{2 \times 1.01 \times 100 \times \dot{n}_{out,dry} \times y_{H_2}}{n_{HAC,in} \times 60.06}$$

Equation 3 Hydrogen Purity (% Dry basis)

$$\text{Hydrogen Purity (\% db)} = \frac{\text{molar rate of hydrogen detected in process gas output}}{\text{total dry gas molar rate detected} - \text{molar rate of } N_2} \times 100$$

Selectivity to carbon gases in the SS period was also calculated from the gas compositions as described in Equation 4;

Equation 4 Selectivity to C-gases

$$sel_{i,C}\% = 100 \times \frac{\alpha_i y_{i,C}}{\sum_j^n \alpha_{j,C} y_{j,C}}$$

The calculated X_{H_2O}, $sel_{i,C}$, hydrogen yield and hydrogen purity were compared with chemical equilibrium and stoichiometric values to ascertain the efficiency of the HAc/steam feed stage.

Further calculations were done to ascertain the cyclic stability and efficiency of the sorbent; the rate of adsorption of CO_2 ($\check{n}_{CO_{2,CARB}}$) was calculated using a carbon balance (Equation 5 A). An integration of the calculated rate was in turn used to derive the percentage conversion of the sorbent material (X_{CO_2}) as detailed in Equation 5B. An efficiency of the sorbent conversion (Eff_{PB} %) was then extrapolated for the different sorption periods using Equation 5C as the example for PB, This was utilised in ascertaining the major share of conversion across the carbonation period.

Equation 5 M rate of carbonation (A), maximum conversion of sorbent per cycle of SE-CLSR (B), and efficiency of conversion (C)

$$\check{n}_{CO_{2,CARB}} = (X_{Hac,ss} \times n \times \check{n}_{Hac,in}) - (\frac{\check{n}_{N_{2,in}}}{y_{N_2,}}(y_{CH_4} + y_{CO_2} + y_{CO}) \text{ (A)}$$

$$X_{CO_2}(\%) = \frac{\int_{t_0}^{t_{ss}} \check{n}_{CO_{2,CARB}} dt}{n_{CaO_{in}}} X\ 100 \text{ (B)}$$

$$Eff_{PB}\ (\%) = \frac{X_{CO_{2,PB}}}{X_{CO_{2,end\ of\ SS}}} \times 100 \text{ (C)}$$

The total carbonation time for each period of the SE-CLSR HAc-steam feed was also determined; t_0, which indicates the beginning of the PB phase was taken from the onset of high hydrogen amount as detected by the micro–GC, whilst t_{BT} and t_{SS} were taken from the time of the onset of CO_2 production and stable CO_2 production respectively.

$\check{n}_{NiO \rightarrow Ni,ss}$ was also calculated as detailed in previous work [54] using Equation 6 where the first part of the equation corresponds to the maximum stoichiometric value when only hydrogen gas is produced alongside solid $CaCO_3$, and the second part of the equation corresponds to the molar rate of produced hydrogen. Integration of $\check{n}_{NiO \rightarrow Ni,ss}$ is used to determine the total moles of reduced nickel, n_{ni}, which in turn can be used to determine the time to full reduction of NiO to Ni (t_{FR}). The ratio of $\check{n}_{NiO \rightarrow Ni,ss}$ to the maximum stoichiometric reduction rate attainable as prescribed by Equation 6C (R_{red}) also aids the discussion of the more dominant reaction in the PB period.

Equation 6 Reduction rate of catalyst for SE-CLSR (A) and time for full reduction of Catalyst (B)

$$\check{n}_{NiO \rightarrow Ni,ss} = \check{n}_{Hac,in} X_{Hac,SS} (2n + 0.5m - k) - y_{H_{2,SS}} \frac{\check{n}_{N_{2,in}}}{(1 - y_{H_{2,SS}})} \text{ (A)}$$

$$t_{FR} = \frac{n_{ni}}{\check{n}_{NiO \rightarrow NiPB}} \text{ (B)}$$

$$R_{red} = 100 \times \frac{\check{n}_{NiO \rightarrow Ni,PB}}{\check{n}_{Hac,in} X_{Hac,SS} (2n + 0.5m - k)} \text{ (C)}$$

In the air feed stage, the dry gas molar flow rate ($\dot{n}_{out,dry}$) realised from nitrogen balance was used to calculate the rate of gasification of the carbon deposited during the previous HAc-steam feed ($\dot{n}_{c,gas}$), using a carbon balance respectively as detailed in Equation 7. The integration of the calculated rate over time gave the total number of moles carbon gasified (n_{Cgas}) during the oxidation step under periodic air feed.

Equation 7 Rate of Carbon gasified

$$(\dot{n}_{c,gas}) = \dot{n}_{out,dry} \times (y_{CO} + y_{CO_2})$$

Chemical equilibrium calculations for the reactive systems chosen in the experiments were derived from outputs of the Chemical Equilibrium with Applications (CEA) software [59]. The software was used to obtain equilibrium values for the process output using the set conditions for the experimental runs (P = 1 bar, T = 650 °C, Omit = C(gr), H_2O(cr) H_2O(l)). The CEA inputs were done assuming 2 systems simulating the two periods; carbonation (PB and BT) (with CaO input) to show sorption activity, and non-carbonation (SS), without CaO input, to compare H_2 yields and purities when the sorbent is active with when it is fully saturated. The input of CaO in the CEA software for the pre-breakthrough phase was calculated from the overall stoichiometric equation on mol basis ($1C_2H_4O_2 = 2CaO$) with the general assumption that all CO_2 produced in the reforming and auto-reduction reactions would be adsorbed by the CO_2 sorbent and converted into $CaCO_3$ in the pre-breakthrough period. The gas compositions derived from the CEA were in turn used to calculate the process outputs at equilibrium using Equation 1–5 by replacing the relevant molar flow rates in the reactor with just molar outputs predicted at equilibrium at same conditions.

3. Results and discussion

3.1. Process outputs with time on stream and upon redox cycling of SE-CLSR-HAc

The three periods of the SE-CLSR fuel-steam feed stage were observed, as illustrated in Fig. 2A, and could be easily identified for all 20 cycles conducted. This also indicated sorption activity during the NiO reduction for all cycles of SE-CLSR.

The air feed step in the SE-CLSR process was used to burn off carbon deposits from the preceding fuel and steam-feed stage, oxidise the catalyst (Ni to NiO) and regenerate the sorbent. The product gas composition as detected by the micro-GC for all 19 SE-CLSR air feed stage (Fig. 2B) contained O_2, CO and CO_2. The exothermic nature of the oxidation process also led to an increase in temperature observed from the Pico log reader at the beginning of the air feed stage for all consecutive 19 air feeds; the increase in temperature varied from cycle to cycle but was within 25 °C to 45 °C for all 19 cycles.

3.1.1. Process Outputs with time on stream- HAc-steam feed stage

Analysis of the process outputs at steady state post breakthrough was used to check the stability of the catalyst after the saturation of the sorbent. The gases monitored by the micro-GC during this stage were CO, CO_2, CH_4, C_2H_6, C_3H_8, (the last two always remaining below threshold of detection), H_2, and N_2.

Elemental analysis of the process outputs at the steady state was used to calculate the X_{HAc}, X_{H_2O}, Hydrogen Purity (%), Hydrogen Yield (wt.%) and selectivity to carbon containing gases as seen in Table 1; It can also be deduced from the $sel_{i,C}$% that the major share of C (gas) formed is in the form of CO_2 (68%–81% across all 20 cycles) which indicates that steam reforming and effective water gas shift reactions are dominant, with very little CH_4 formed (< 2% of the gas carbon share for all 20 cycles).

More than 80% of the fuel's carbon was converted to gases across all 20 cycles of SE-CLSR, corresponding to steam conversion X_{H_2O} larger than 75% of the equilibrium and H_2 yield in excess of 78% of the equilibrium. The hydrogen purity across the reducing phase of all cycles of SE-CLSR was also between 92%–95% of the calculated stoichiometric or theoretical maximum which equates to > 97% of the equilibrium value.

The consistent process output analysis in the steady state when the sorbent was saturated over 20 SE-CLSR cycles indicated no loss of catalytic activity across the cycles, this is in accordance and is similar to results from other studies on the SE-CLSR of bio-oils, acetic acid and other model oxygenates of bio-oil [27,28,60].

3.1.2. Overall carbon balance of SE-CLSR process

An overall carbon balance was carried out on the SE-CLSR process across 20 cycles as detailed in Table 2; The carbon evolved out of the process gas in the fuel-feed stage (C-out process) amounted to 47%–86.4% of the total carbon share in the process with the remaining carbon having burnt off during oxidation. Carbon in the condensates was negligible in all cases (< 0.07% of the total carbon share).

The rate and extent of carbonation during the carbonation period (PB and BT) is essential to ascertain efficient sorbent activity during the SE-CLSR process. It is widely reported that the carbonation of the sorbent starts with a fast-chemical carbonation reaction which is then followed by a slower diffusion controlled phase reaction caused by the presence of a $CaCO_3$ barrier layer [27,37,61,62].

The carbonation rate was optimal at the PB phase for all 20 SE-CLSR cycles and was between 7.7×10^{-6} mol/s to 8.87×10^{-6} mol/s. This indicates that the sorbent had the capability to operate with the same intensity for that period across multiple cycles.

There was a gradual decline in the carbonation duration in the PB phase until the 9th cycle where it became steady between 12 min. to

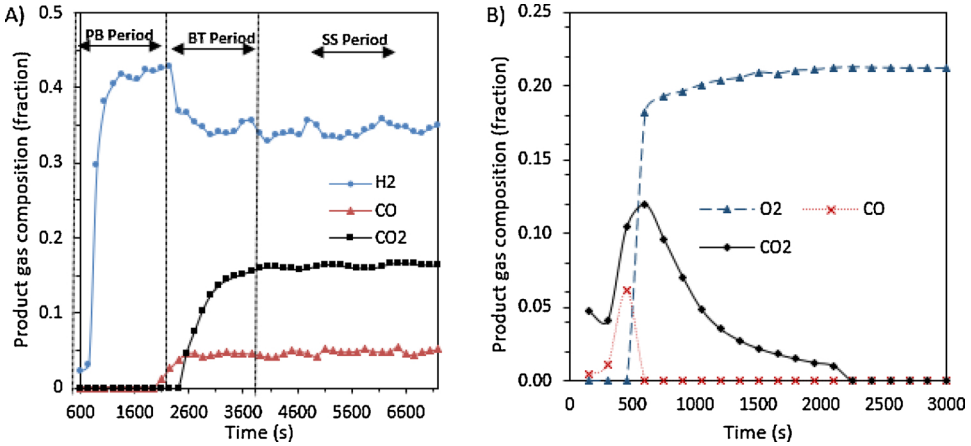

Fig. 2. Dynamic profile of process gas composition (dry basis) (A): HAc-steam feed with T_{SR} = 650 °C, WHSV = 1.18 h^{-1}, S/C = 3, (B): Air feed with T_{OX} = 850 °C, T_{HY} = 650 °C).

Table 1
Process analysis at steady state or post breakthrough phase (T_{SR} = 650 °C, WHSV = 1.18 h^{-1}, S/C = 3, T_{OX} = 850 °C, T_{HY} = 650 °C).

cycle number	X_{HAc} (frac) Equation 1	X_{H2O} (frac)	H_2 Purity (%) Equation 3	H_2 Yield (Wt. %) Equation 2	$sel_{CO2,C}$% Equation 4	$sel_{CO,C}$%	$sel_{CH4,C}$
1	0.92	0.20	61.93	10.02	77.10	22.40	0.50
2	0.81	0.18	63.14	8.93	80.60	18.40	0.90
3	0.81	0.19	62.48	9.09	81.00	17.60	1.40
4	0.84	0.18	61.77	9.10	79.70	18.40	1.90
5	0.83	0.20	63.12	9.52	81.10	17.80	1.10
6	0.87	0.20	62.38	9.71	80.00	18.45	1.55
7	0.92	0.20	61.64	9.90	78.90	19.10	2.00
8	0.90	0.19	61.34	9.54	78.80	19.60	1.60
9	0.87	0.20	62.58	9.73	80.50	18.40	1.00
10	0.86	0.19	62.07	9.42	79.30	20.00	0.80
11	0.85	0.20	62.71	9.56	80.30	19.00	0.70
12	0.86	0.19	62.30	9.71	76.10	23.30	0.60
13	0.88	0.20	62.29	9.80	78.50	21.10	0.50
14	0.88	0.19	62.03	9.60	76.90	22.60	0.50
15	0.91	0.20	63.14	9.92	68.10	30.20	1.70
16	0.90	0.21	62.81	10.25	79.90	19.80	0.30
17	0.86	0.19	62.27	9.62	76.60	22.80	0.60
18	0.92	0.19	61.57	9.90	74.40	25.10	0.60
19	0.90	0.21	62.71	10.23	80.30	19.50	0.30
20	0.94	0.21	63.14	10.39	75.00	24.40	0.60
Equilibrium		0.24	63.14	11.53	77.10	22.40	0.50
Stoic			66.60	13.38			

13 min. of time on stream; the reduction in the pre-breakthrough period can be attributed to a change in kinetics and CO_2 capture which would have an effect on the full efficiency of the sorbent and its sorption enhancement capabilities [27].

There is also a decline in the total carbonation time (t_{PB} + t_{BT}) in the first few SE-CLSR cycles; this corresponds to a decrease in n_{Cgas} of the air feed and an increase in the C-out from the process gas in the fuel-feed stage as seen in Fig. 3. This supports a gradual decrease in the CO_2 captured during the fuel-feed stage. This also indicates that the PB period plays a greater influence in the sorbent conversion and efficiency as an increase in the carbonation duration propelled during the BT period does not lead to a decrease in C-out from the process gas in the fuel-feed stage.

A comparison of the share of carbon in the 1st five SE-CLSR cycles with the corresponding process without sorption activity (CLSR) can be seen in Fig. 4; the carbon content from the process gas has more influence in the CLSR experiments where it averaged 89% when compared to SE-CLSR experiments where it averaged 53% across the first 5 cycles. This is attributed to sorption activity in the SE-CLSR experiments which ensures that part of the carbon generated during the reforming phase would be captured by the sorbent. This led to an increase in the carbon gases generated during the air feed stage of SE-CLSR due to the release of the captured carbon during calcination of the sorbent as expected.

3.1.3. Sorption enhancement capacity and conversion at PB phase across 20 cycles of SE-CLSR

Sorption enhancement has been promoted to improve the efficiency of the steam reforming process. The calculated hydrogen purity in the PB period was > 96 vol% across all 20 cycles of SE-CLR; this is way higher than values realised after the saturation of the sorbent which was in average 62% across all cycles.

Table 2
Overall Carbon balance of SE-CLSR process (T_{SR} = 650 °C, T_{OX} = 850 °C, WHSV = 1.18 h^{-1}, S/C = 3, T_{HY} = 650 °C).

	C in feed (Mol) during HAc/steam feed	X_{HAc} (%) Equation 1	C- out Process (mol)	n_{Cgas} (mol) during air feed Equation 7	C- condensate (mol)	Total carbon out (mol)	Carbonation time (PB) (s)	**$Nco_{2,\ CARB,PB}$ (mol/ s)** Equation 5
1	6.91×10^{-2}	91.76	3.91×10^{-2}	3.09×10^{-2}	5.13×10^{-5}	7.00×10^{-2}	1650	8.70
2	6.91×10^{-2}	80.90	3.13×10^{-2}	3.51×10^{-2}	2.00×10^{-5}	6.65×10^{-2}	1650	7.67
3	6.91×10^{-2}	81.10	3.15×10^{-2}	3.56×10^{-2}	0.85×10^{-5}	6.71×10^{-2}	1350	7.66
4	6.91×10^{-2}	83.91	3.74×10^{-2}	2.87×10^{-2}	1.86×10^{-5}	6.61×10^{-2}	1200	7.88
5	6.91×10^{-2}	82.89	3.84×10^{-2}	4.31×10^{-2}	1.94×10^{-5}	8.15×10^{-2}	1200	7.82
6	6.91×10^{-2}	87.35	3.26×10^{-2}	3.54×10^{-2}	1.87×10^{-5}	6.80×10^{-2}	1050	8.05
7	6.91×10^{-2}	91.81	4.20×10^{-2}	2.71×10^{-2}	1.98×10^{-5}	6.92×10^{-2}	900	8.70
8	6.91×10^{-2}	89.56	3.58×10^{-2}	3.15×10^{-2}	1.42×10^{-5}	6.73×10^{-2}	900	8.45
9	6.91×10^{-2}	86.72	3.24×10^{-2}	2.93×10^{-2}	2.29×10^{-5}	6.17×10^{-2}	750	8.19
10	6.91×10^{-2}	85.77	4.11×10^{-2}	2.81×10^{-2}	1.90×10^{-5}	6.92×10^{-2}	750	8.12
11	6.91×10^{-2}	84.62	3.56×10^{-2}	2.98×10^{-2}	1.54×10^{-5}	6.54×10^{-2}	600	8.00
12	6.91×10^{-2}	86.01	3.87×10^{-2}	3.24×10^{-2}	2.75×10^{-5}	7.12×10^{-2}	600	8.15
13	6.91×10^{-2}	88.44	3.61×10^{-2}	2.82×10^{-2}	1.69×10^{-5}	6.44×10^{-2}	750	7.88
14	6.91×10^{-2}	87.58	3.82×10^{-2}	2.64×10^{-2}	1.95×10^{-5}	6.46×10^{-2}	750	8.29
15	6.91×10^{-2}	91.24	3.91×10^{-2}	2.17×10^{-2}	1.98×10^{-5}	6.08×10^{-2}	750	8.65
16	6.91×10^{-2}	90.45	4.71×10^{-2}	1.67×10^{-2}	3.81×10^{-5}	6.38×10^{-2}	600	8.56
17	6.91×10^{-2}	86.84	4.77×10^{-2}	1.94×10^{-2}	3.66×10^{-5}	6.71×10^{-2}	600	8.22
18	6.91×10^{-2}	92.06	3.57×10^{-2}	2.43×10^{-2}	2.61×10^{-5}	6.00×10^{-2}	600	8.67
19	6.91×10^{-2}	90.68	4.43×10^{-2}	1.81×10^{-2}	3.06×10^{-5}	6.25×10^{-2}	600	8.59
20	6.91×10^{-2}	93.69	5.60×10^{-2}	0.87×10^{-2}	2.90×10^{-5}	6.48×10^{-2}	600	8.87

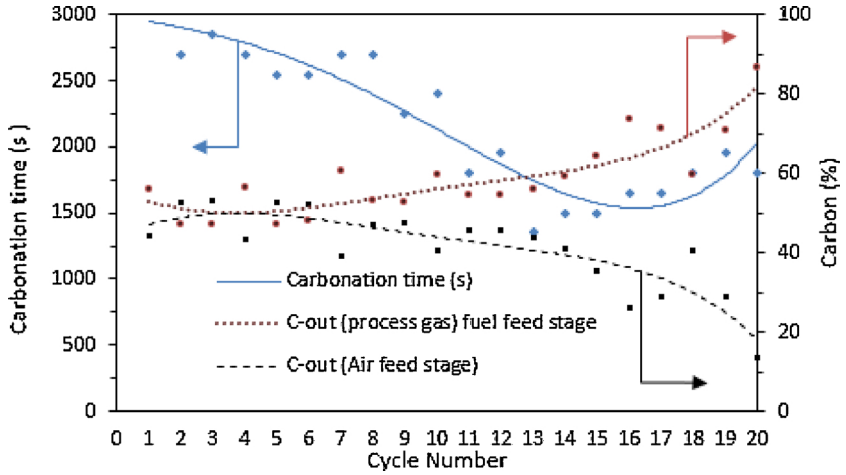

Fig. 3. Total carbonation duration and the share of carbon across the cycles of SE-CLSR. Lines are polynomial fits applied to relevant experimental data. (T_{SR} = 650 °C, WHSV = 1.18 h^{-1}, S/C = 3, T_{OX} = 850 °C, T_{HY} = 650 °C).

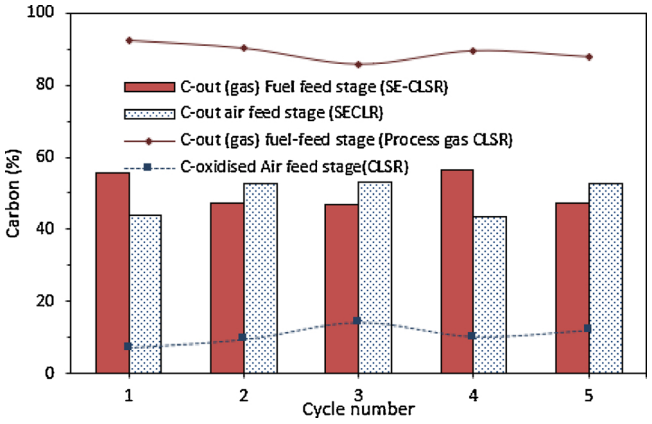

Fig. 4. % carbon share in CLSR and SE-CLSR experiments across 5 cycles (T_{SR} = 650 °C, WHSV = 1.18 h^{-1}, S/C = 3, T_{OX} = 850 °C, T_{HY} = 650 °C).

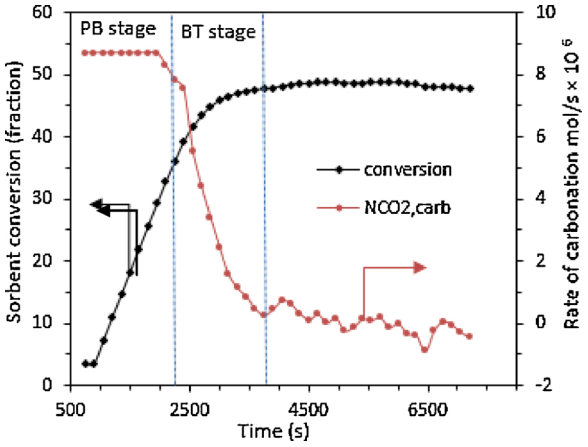

Fig. 5. Sorbent conversion (%) and carbonation rate (mol/s) during the 1st cycle of SE-CLSR of acetic acid (T_{SR} = 650 °C, WHSV = 1.18 h^{-1}, S/C = 3, T_{OX} = 850 °C, T_{HY} = 650 °C).

The auto-reduction of the catalyst typical of chemical looping steam reforming also occurs prominently in the PB period; across all 20 SE-CLSR cycles, the maximum time estimated for the catalyst reduction was between 8 −11 min, this corresponds to a $\%R_{red}$ between 39%–44% across the cycles. This confirms that sorption enhanced steam reforming reactions were prominent alongside NiO reduction during pre-breakthrough.

One of the major challenges associated with sorption enhanced processes is the sorbent deactivation that occurs across the cycles, this can be monitored by sorbent conversion and the rate of carbonation per cycle (Fig. 5). The major share of sorbent conversion (calculated using Equation 5) occurred in the PB period across all 20 cycles of SE-CLSR of acetic acid; > 50% of the sorbent was converted during PB across all 20 cycles with over 80% sorbent conversion occurring in the first two SE-CLSR cycles. This indicates that most of the sorbent converted would have efficiently occurred during the production of high purity hydrogen (> 96% dry basis for all 20 cycles).

As detailed earlier in Table 2, there was no decline in the $\check{n}_{CO_2,CARB}$ across the cycles, however there was an observed drop in the efficiency of conversion in the PB period particularly in the first few cycles. It is essential to stress that the total efficiency for the overall process > 83% accross all 20 cycles, this is due to the increase in the role played by the BT phase as seen in Fig. 6A. It is also apparent from Fig. 6B that the drop in the sorbent conversion had no bearing on the conversions of either the HAc or the steam which indicates that the catalyst operated efficiently across the cycles even as deactivation of the sorbent occurred.

An overall conversion efficiency was calculated to have a more precise idea of the deactivation of the sorbent across the SE-CLSR cycles as depicted in Fig. 6C; it is generally agreed and reported that the conversion fraction is realistically optimal between 0.45 - 0.50 due to conversion limitations caused by pore filling and pore blockage of calcined limestone which is microporous in nature [63]. The overall efficiency for this study was calculated on the assumption that maximum conversion occurs and is optimal at the first SE-CLSR cycle (0.48) using Equation 8;

Equation 8 Overall conversion of sorbent

$$\textit{Overall conversion efficiency at cycle X} = \left(\frac{\textit{conversion fraction at cycle X}}{\textit{maximum conversion fraction} = 0.48}\right) \times 100$$

The decay in the conversion fraction across the 20 cycles of SE-CLSR can be seen in Fig. 6C; it can be observed that the overall conversion efficiency or sorption activity for the activated sorbent declines steadily until it stabilises from the 11th cycle. A similar trend for maximum conversion fraction has been observed in previous work on the cyclic ability or stability of CaO sorbent [64]; at the end of the 20th cycle the sorbent conversion efficiency had dropped to approximately 50% of the overall conversion efficiency obtained at the end of the first cycle. This corresponds to 26% – 34% conversion efficiency obtained at the pre-breakthrough period from the end of the 9th cycle to the 20th cycle from

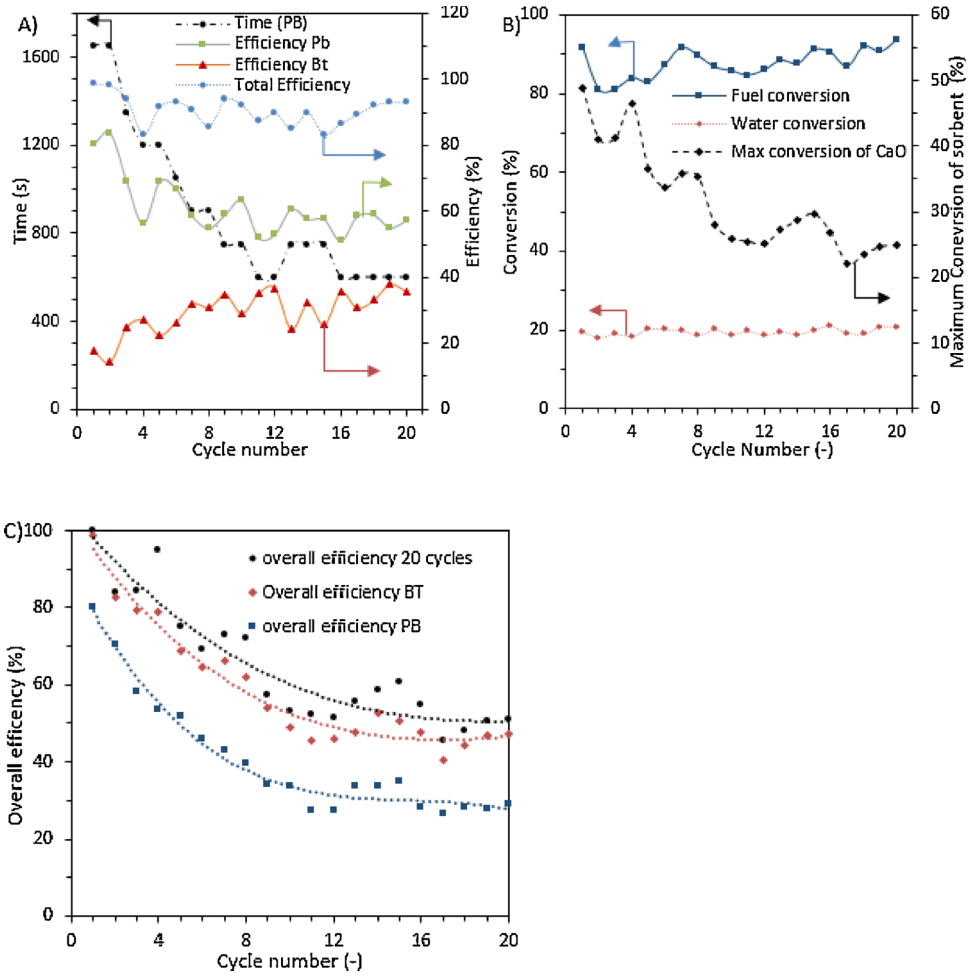

Fig. 6. Sorbent efficiency across 20 cycles of SE-CLSR (T_{SR} = 650 °C, WHSV = 1.18 h^{-1}, S/C = 3, T_{OX} = 850 °C, T_{HY} = 650 °C) A: Efficiency of sorbent conversion and carbonation duration, B: sorbent conversion, water and fuel conversion C: Overall sorbent conversion efficiency across all cycles (Lines are polynomial fits applied to relevant experimental data).

80% obtained at the end of the 1st cycle.

3.1.4. SE-CLSR solids and condensates characterisation

The major reactions occurring at the fuel-feed stage are carbonation of the calcined sorbent, auto-reduction of catalyst and steam reforming; A loss in overall surface area and porosity as seen in Table 3 is observed when the materials after use in conventional steam reforming are compared to those following cycling during SE-CLSR. This is attributed to sorbent decay and suggests that the deterioration in sorbent conversion over repeated cycles can be related to the loss of surface area and pore characteristics as already inferred in previous studies [27], and exacerbated by sintering during the oxidation phase which was carried out at a set temperature of 850 °C to ensure optimal calcination of the sorbent but would likely have featured bouts of exothermicity during nickel oxidation and carbon burn-out. Also, as observed in Table 3, there is a similar pore volume and surface area of the used oxidised solid materials when compared to its reduced forms after several cycles. This is because the Red-Ox cycles would ensure stability of the Ni particle size and activity [65]

The effect of the loss in surface area and porosity resulting from the oxidation stage is corroborated in Table 3 which indicates a 71% loss in surface area and a 24% loss of pore volume when the fresh solid material (oxidised) is compared to the oxidised used material after 8 cycles; the loss of surface area and porosity is attributed to both catalysts and sorbent activities.

It can therefore be inferred and assumed from the comparison of the surface area that there would be a reduction in the MBET surface area of the sorbent plus catalyst across the cycles which would affect the sorbent conversion in the next cycle until a certain point when the surface area becomes steady due to the Red-Ox cycling just as observed in the overall efficiency of the sorbent. There is however, a reduction in

Table 3
BET surface area analysis of SE-CLSR process (T_{SR} at 650 °C, T_{OX} 850 °C, S/C = 3). Catalyst (Red) + sorbent ($CaCO_3$) indicates the analysis was carried out after a reduction/steam reforming under HAc and steam feed, and prior to the oxidation stage under air feed. Oxidised catalyst + calcined sorbent indicates an analysis performed on bed materials subsequent to an air feed stage.

	MBET surface area m^2/g	Pore volume cm^3/g	Pore radius nm
Catalyst (Red) + activated sorbent (calcined) Fresh	17.5	0.097	1.90
Catalyst (Red) + sorbent ($CaCO_3$) after SE-Steam Reforming	20.3	0.067	1.91
Catalyst (Red) + sorbent ($CaCO_3$) after 10 cycles of SE-CLSR	10.7	0.054	1.90
Catalyst (Red) + sorbent ($CaCO_3$) after 20 Cycles of SE-CLSR	13.4	0.055	0.95
Fresh Catalyst (oxidised form) + activated sorbent (calcined)	33.7	0.076	1.92
Oxidised catalyst + calcined sorbent (after 8 cycles of SE-CLSR)	9.6	0.058	1.86

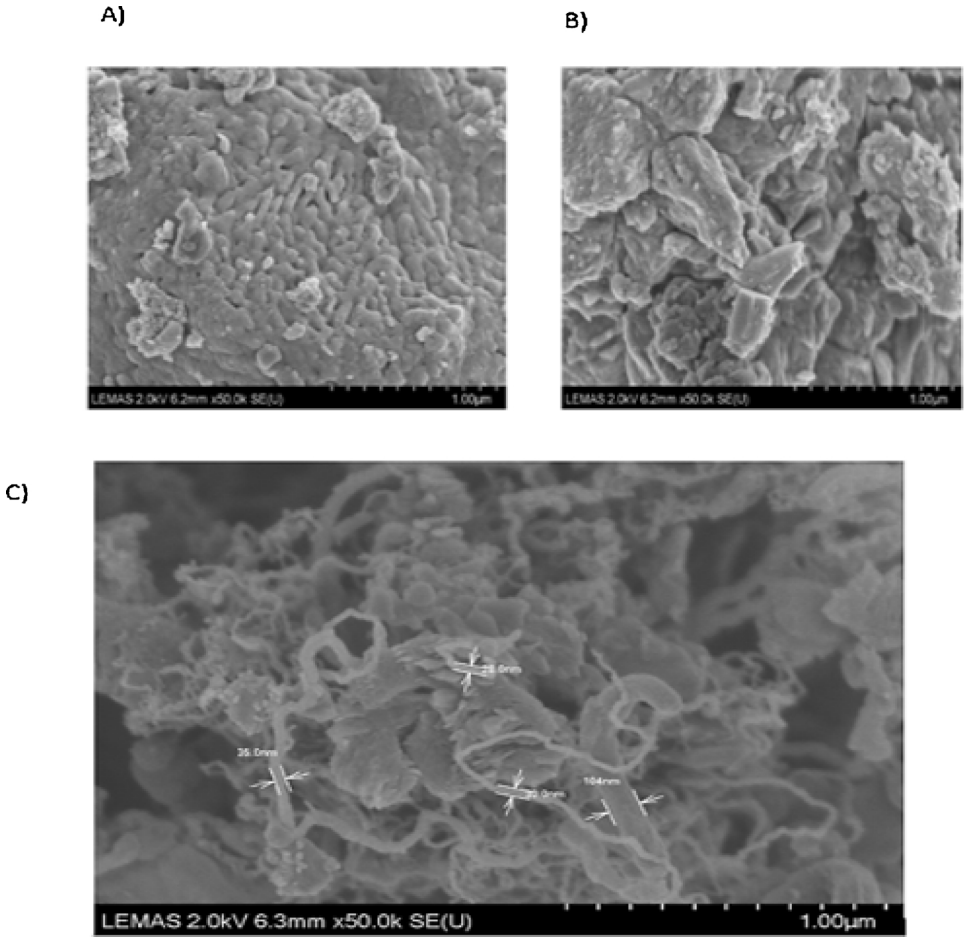

Fig. 7. SEM images of the A) fresh catalyst (oxidised) mixed with calcined sorbent B) Used catalyst (oxidised) mixed calcined sorbent C) used catalyst (reduced) and sorbent ($CaCO_3$) after 20 cycles of SE-CLSR of acetic acid (T_{SR}: 650 °C, T_{OX}: 850 °C, S/C:3).

the pore radius of the used catalyst and sorbent mix from cycle to cycle which indicates the formation of smaller pores.

SEM images of the fresh and used catalyst plus sorbent can be seen in Fig. 7; a similar image can be seen for the oxidised and fresh catalyst plus sorbent, filamentous carbon cannot be noticed in the oxidised material when compared to the used catalyst and sorbent. Two types of carbon filaments were observed in Fig. 7C on the used catalyst, large carbon filaments of about 139 nm and shorter ones in the 19–35 nm range; it has been inferred that the carbon formed could also be deposited on the surface of the sorbent [60], these, as seen in the SEM images of the oxidised materials, would be burnt off during oxidation.

TEM and SAED patterns indicates the presence of filamentous carbon formed on the materials as seen in Fig. 8A. A detailed poly crystalline structure can be observed in Fig. 8B, while amorphous carbon (Fig. 8C and D) is also formed. This is similar to TEM results detailed for CLSR without sorption enhancement as detailed in previous studies [54].

The metal ion concentration of the collected condensate indicates the presence of Ni in the condensate, which suggests some leaching during the SE-CLSR; It can be observed that the Ni concentration present in the condensates collected after 20 cycles of sorption enhanced reforming is higher than that present in the other tested condensates however, this amounts to 0.06% of the nickel present in the cycle and is therefore taken as insignificant.

3.2. SE-CLSR with T_{HY} at 250 °C

Pre-hydration of sorbents has been promoted to increase the reactivity of the CaO sorbents and improve its conversion over repeated carbonation-calcination cycles [52]; the T_{HY} utilised alongside the calcination temperature has also been shown to have a huge impact on the hydration extent of the sorbent particularly in cases where carbonation of the sorbent occurs immediately after hydration (direct hydration) [53]. In previous SE-CLSR runs already discussed, steam was introduced into the catalyst and sorbent mix at 650 °C before acetic acid was introduced. This was done with the intent to further gasify any residual carbon that was not oxidised during the air feed stage; 5 SE-CLSR cycles were conducted using the same condition utilised for the previous SE-CLSR runs except with the pre-hydration temperature set to 250 °C with nitrogen utilised as inert gas.

3.2.1. Process Outputs with time on stream, HAc-Steam feed stage at T_{HY} set to 250 °C

The three identified phases for SE-CLSR could also be observed easily across all 5 cycles of SE-CLSR with pre-hydration at 250 °C.

However, in excess of 97% of the fuel was converted across all 5 cycles of SECLR which also corresponded to more than 97% yield of hydrogen when compared to equilibrium values. As detailed in Fig. 9, this is higher than the values observed in the SE-CLSR experiments with T_{HY} set to 650 °C. There was an identified increase in the $sel_{CO_2,C}$% and $sel_{CH_4,C}$% seen in the SE-CLSR runs when T_{HY} is set to 250 °C compared to those done at 650 °C.

This exemplifies that there might be a better reaction dynamic in the SE-CLSR with T_{HY} set to 250 °C still apparent even after the saturation of the sorbent; The increased sorption activity in this set of experiments would have led to an increase in the dynamics of reactions producing

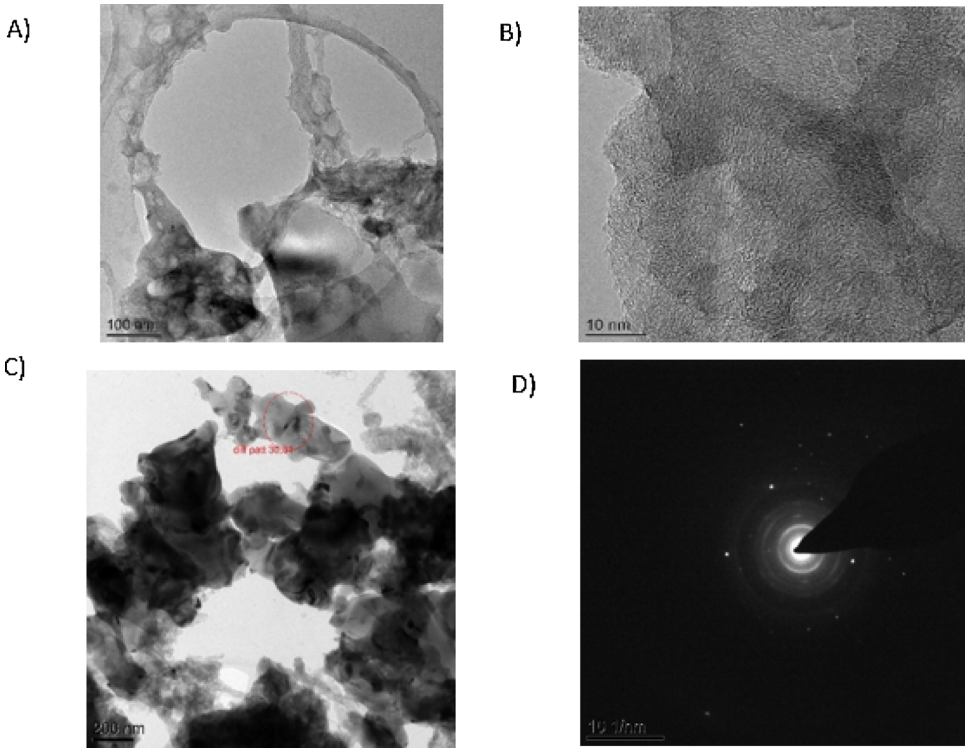

Fig. 8. TEM images (8 A, 8B and 8C) and Diffraction pattern (8D) of used SE-CLSR material (in reduced form) after 10 cycles of reforming; T_{SR} = 650 °C, T_{OX} = 800 °C, catalyst B, WHSV = 2.5 h^{-1}, S/C = 3 A-.

carbon-dioxide which is not limited to steam reforming and water gas shift reactions alone but also include side reactions like carbon gasification and acetic acid decomposition.

3.2.2. Process output analysis at PB period with T_{HY} set to 250 °C

There is no observed reduction in the $\check{n}_{CO_2,CARB}$ and carbonation duration the PB period across the SE-CLSR cycles with T_{HY} set to 250 °C as detailed in Table 4; there is however a shorter carbonation period when compared with the SE-CLSR experiments with T_{HY} set to 650 °C. This can be attributed to the increase in the carbonation rate observed in the cycles with hydration set to 250 °C. An average pre-breakthrough carbonation rate of 9.46 × 10^{-6} mol/s was derived across the SE-CLSR cycles with hydration temperature set to 250 °C which is 20% higher than the 7.94 × 10^{-6} mol/s calculated for the first 5 SE-CLSR cycles with hydration temperature set to 650 °C. The increased rate would have led to a quicker saturation of the sorbent which consequently would reduce the carbonation period.

Regarding the conversion of the sorbent, the maximum conversion of CaO remained relatively stable between 43% and 46% across the 5 cycles of SE-CLSR cycles; this corresponds to a stable conversion efficiency > 96% across all 5 cycles. As detailed in Fig. 10A, the conversion of the sorbent in the PB phase accounted for > 73% of the total sorbent conversion, this was similar to the results obtained with T_{HY} at 650 °C.

However, it is essential to note that sorbent conversion in the PB period was more efficient in the subsequent cycles with T_{HY} at 250 °C (in average 77% in cycles 2–5) compared to values at T_{HY} of 650 °C (69% in cycles 2–5). Fig. 10B further shows that the drop in sorbent conversion across the SE-CLSR cycles with T_{HY} at 650 °C over both PB and BT periods was not prevalent with T_{HY} at 250 °C. This indicates that the sorbent converted more efficiently in the SE-CLSR cycles with the lower T_{HY}.

The reduction of the catalyst is also of interest in SE-CLSR as the reduction of the nickel oxide to nickel also produces CO_2 and hence in situ CO_2 capture would be expected to promote it via both equilibrium shift, and augmented kinetic rates resulting from higher partial pressures of gas reactants. Fig. 11B shows that the NiO-Ni rate was higher in the SE-CLSR runs with T_{HY} 250 °C than with T_{HY} 650 °C (in average 8.31 × 10^{-6} mol/s compared to 6.36 × 10^{-6} mol/s). This was still higher than the corresponding NiO-Ni rate obtained in the experiments without sorption which averaged 1.28 × 10^{-6} mol/s across 5 cycles of CLSR. It can also be ascertained from Table 4 that reduction of the catalyst occurred completely in the PB phase with a similar % R_{Red} observed for the SE-CLSR runs with T_{HY} set at 250 °C and at 650 °C. This, as indicated in Fig. 11 was much higher than in the experiments without sorption. This shows that SESR and, what we term here and observe for the first time "sorption enhanced catalyst auto-reduction" or "SECAR" would have occurred concurrently in the PB phase.

An advantage of hydration of the sorbent is to improve the conversion of the sorbent across the cycles, allowing the sorbent to reach closer to its theoretical capacity for CO_2 capture; The sorbent conversion by the end of the 5 SE-CLSR cycles with T_{HY} at 250 °C was > 96% when compared to the 1st cycle whereas there is a decay in the sorbent conversion of the SE-CLSR cycles with T_{HY} set to 650 °C to 75% when compared to the 1st cycle (Fig. 6).

4. Conclusion

The efficiency of SE-CLSR of acetic acid was investigated with the view to determine the cyclic ability and stability of CaO based sorbents and the overall effect of CO_2 sorption on the chemical looping steam reforming of acetic acid, as model bio-compound for biomass pyrolysis oils.

Sorption enhanced, sustained steam reforming was observed for all 20 cycles of SE-CLSR with an average estimated fuel conversion of 88%. An overall carbon balance also indicated that the major share of carbon utilised was either released as C-containing gases or burnt off/desorbed as CO_2 in the oxidation phase.

However, there was an observed drop in sorbent conversion notably in the pre- breakthrough period, and by the end of the 20th cycle, the conversion efficiency had dropped 50% from its initial value. This is

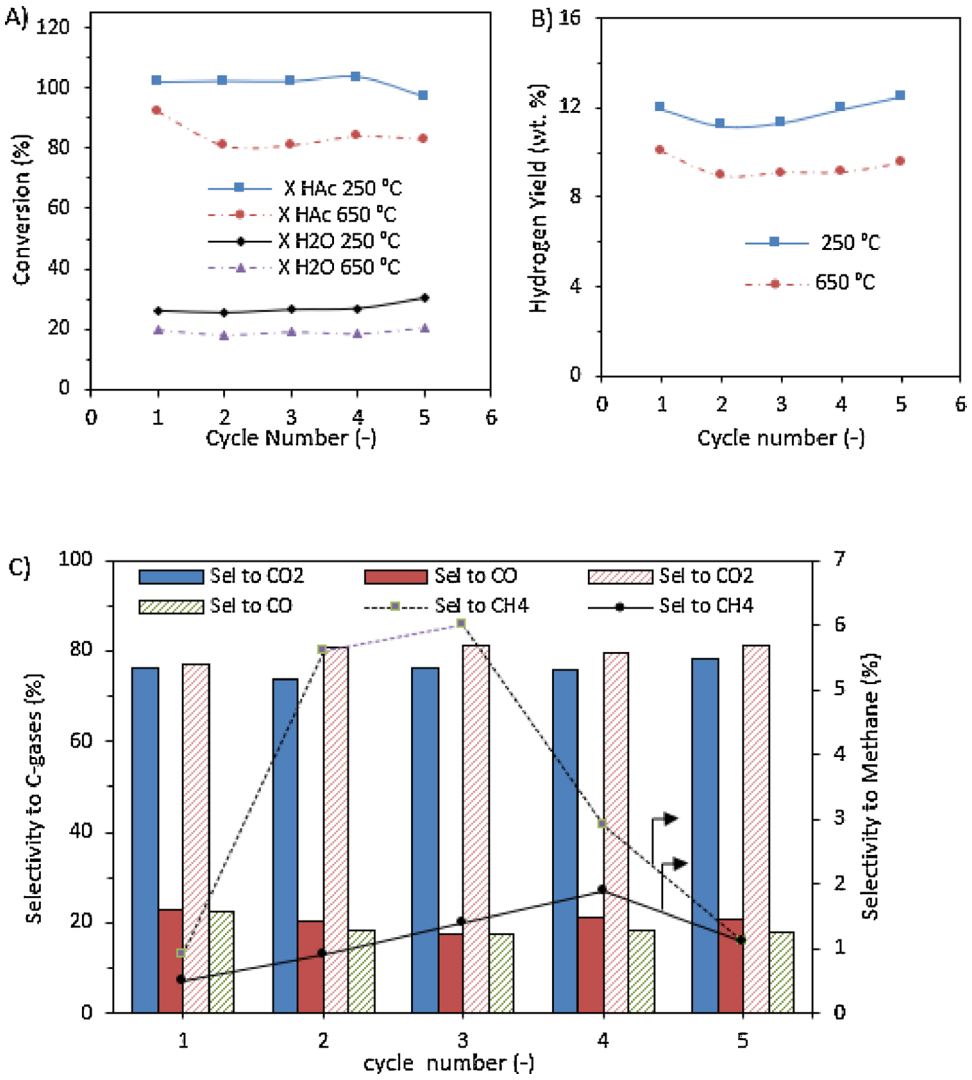

Fig. 9. A) Conversion (%), B) Hydrogen yield of SE-CLSR, and C) selectivity to carbon gases with pre-hydration set at 250 °C and 650 °C (T_{SR} = 650 °C, WHSV = 1.18 h^{-1}, S/C = 3, T_{OX} = 850 °C).

consistent with the literature on cyclic CaO sorption of CO_2, and has been attributed to reduced porosity and sintering of the material [36,37]. This prompted the need for trying reactivation techniques to mitigate the decay of the CaO sorbent across redox cycling of chemical looping.

Steam hydration of the material is known to improve the reactivity of CaO based sorbents and was carried out T_{HY} at 250 °C. Steam hydration of the sorbent before the fuel feed step facilitated a new significant process we termed here sorption enhanced catalyst auto-reduction or "SECAR". SECAR is brought about by the in-situ capture of CO_2 generated during auto-reduction of the oxygen carrier catalyst via the unmixed combustion reaction. Catalyst auto-reduction is a key feature specific to chemical looping and has been shown to operate with many volatile biomass derived feedstock with nickel reduction on supported catalysts [66,67]. There was also an observed stable sorbent conversion across the cycles of sorption enhanced chemical looping reforming with steam hydration at 250 °C; this further demonstrates that direct steam hydration can be an effective reactivation technique to ensure efficient sorption capabilities and conversion of CaO based sorbents during looping cycles [52,53].

Acknowledgements

The authors would like to acknowledge the Niger Delta

Table 4
Process output analysis of SE-CLSR with T_{HY} = 250 °C (T_{SR} = 650 °C, WHSV = 1.18 h^{-1}, S/C = 3, T_{OX} = 850 °C).

cycle number	PB Carbonation Duration (T_{BT}-T_0) (s)	BT carbonation duration (T_{SS}-T_{BT}) (s)	Total Carbonation Time at SS (s)	$\check{n}_{CO_2,CARB}$ (mol/s) Equation 5	Max conversion of CaO per cycle (%) Equation 5	NiO-Ni rate (mol/s) Equation 6	Time to maximum NiO-Ni reduction (s) Equation 6
1	1050	750	1800	9.66×10^{-6}	44.22	–	–
2	1200	1200	2400	9.57×10^{-6}	44.60	8.97×10^{-6}	448
3	1050	1500	2550	9.33×10^{-6}	44.70	8.94×10^{-6}	449
4	900	1650	2550	9.61×10^{-6}	42.67	8.76×10^{-6}	459
5	1050	1500	2550	9.14×10^{-6}	45.53	6.56×10^{-6}	612

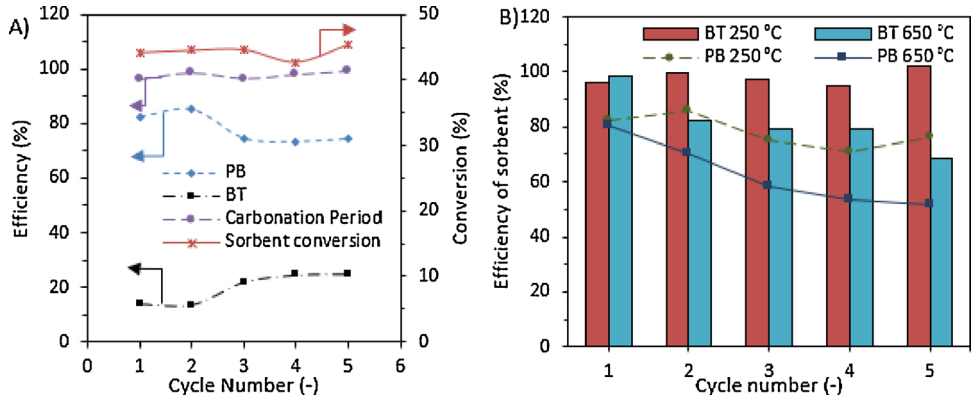

Fig. 10. A) Sorbent conversion efficiency across SE-CLSR cycles with T_{HY} = 250 °C B) comparison of sorbent conversion at T_{HY} = 250 °C and T_{HY} = 650 °C (T_{SR} = 650 °C, WHSV = 1.18 h^{-1}, S/C = 3, T_{OX} = 850 °C).

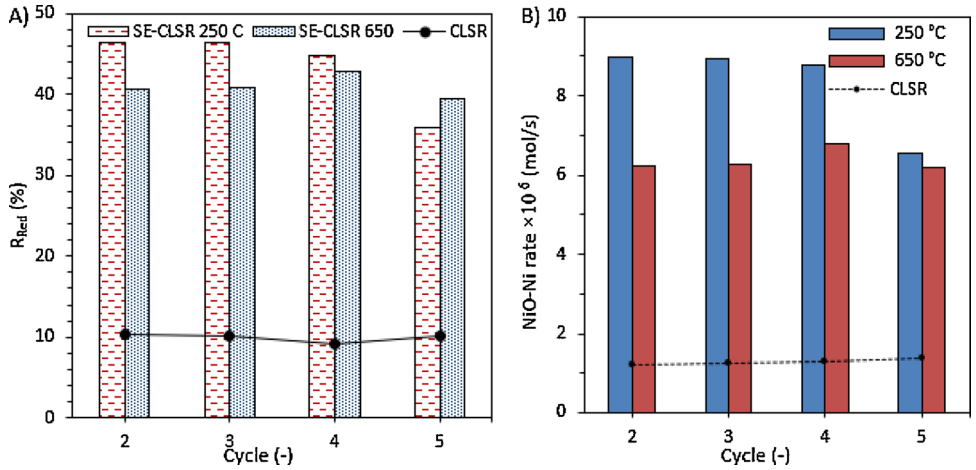

Fig. 11. A) NiO-Ni Reduction rate potential (R_{Red} (%) B) NiO-Ni rate T_{SR} = 650 °C, WHSV = 1.18 h^{-1}, S/C = 3, T_{OX} =. 800–850 °C).

Development Commission (NDDC) Nigeria for financial support of O. Omoniyi's PhD studentship. Martyn V. Twigg at TST Limited is gratefully acknowledged for providing the nickel catalysts. We also acknowledge Longcliffe calcium carbonates for providing the sorbent. We also thank the EPSRC for the consortium grant "SUPERGEN: Delivery of Sustainable Hydrogen" (EP/G01244X/1).

References

[1] J. Ogden, C. Yang, J. Cunningham, N. Johnson, X. Li, M. Nicholas, N. Parker, Y. Sun, J.O.a.L. Anderson (Ed.), Sustainable Transportation Energy Pathways, Institute of Transportation Studies, University of California, Davis, 2011, pp. 64–95.
[2] P. Mohanty, K.K. Pant, R. Mittal, Wiley Interdiscip. Rev. Energy Environ. 4 (2015) 139–155.
[3] D.B. Levin, R. Chahine, Int. J. Hydrogen Energy 35 (2010) 4962–4969.
[4] P.C. Hallenbeck, M. Abo-Hashesh, D. Ghosh, Bioresour. Technol. 110 (2012) 1–9.
[5] J. Fermoso, F. Rubiera, D. Chen, Energy Environ. Sci. 5 (2012) 6358–6367.
[6] G. Nahar, V. Dupont, M.V. Twigg, E. Dvininov, Appl. Catal. B Environ. 168–169 (2015) 228–242.
[7] R. Trane, S. Dahl, M. Skjøth-Rasmussen, A. Jensen, Int. J. Hydrogen Energy 37 (2012) 6447–6472.
[8] E.C. Vagia, A.A. Lemonidou, Appl. Catal. A Gen. 351 (2008) 111–121.
[9] D. Wang, S. Czernik, E. Chornet, Energy Fuels 12 (1998) 19–24.
[10] J.R. Galdámez, L. García, R. Bilbao, Energy Fuels 19 (2005) 1133–1142.
[11] F. Bimbela, M. Oliva, J. Ruiz, L. García, J. Arauzo, J. Anal. Appl. Pyrolysis 79 (2007) 112–120.
[12] K. Takanabe, K.-i. Aika, K. Seshan, L. Lefferts, J. Catal. 227 (2004) 101–108.
[13] A. Basagiannis, X. Verykios, Appl. Catal. A Gen. 308 (2006) 182–193.
[14] D. Wang, D. Montane, E. Chornet, Appl. Catal. A Gen. 143 (1996) 245–270.
[15] P.N. Kechagiopoulos, S.S. Voutetakis, A.A. Lemonidou, I.A. Vasalos, Energy Fuels 20 (2006) 2155–2163.
[16] P. Pimenidou, G. Rickett, V. Dupont, M. Twigg, Bioresour. Technol. 101 (2010) 6389–6397.
[17] V. Dupont, A. Ross, I. Hanley, M. Twigg, Int. J. Hydrogen Energy 32 (2007) 67–79.
[18] V. Dupont, A. Ross, E. Knight, I. Hanley, M. Twigg, Chem. Eng. Sci. 63 (2008) 2966–2979.
[19] R.M. Zin, A. Ross, J. Jones, V. Dupont, Bioresour. Technol. 176 (2015) 257–266.
[20] B. Dou, H. Zhang, G. Cui, Z. Wang, B. Jiang, K. Wang, H. Chen, Y. Xu, Int. J. Hydrogen Energy 42 (2017) 26217–26230.
[21] R.M. Zin, A. Lea-Langton, V. Dupont, M.V. Twigg, Int. J. Hydrogen Energy 37 (2012) 10627–10638.
[22] M.V. Gil, J. Fermoso, C. Pevida, D. Chen, F. Rubiera, Appl. Catal. B Environ. 184 (2016) 64–76.
[23] M.V. Gil, J. Fermoso, F. Rubiera, D. Chen, Catal. Today 242 (2015) 19–34.
[24] G. Esteban-Díez, M.V. Gil, C. Pevida, D. Chen, F. Rubiera, Appl. Energy 177 (2016) 579–590.
[25] R. Hu, D. Li, H. Xue, N. Zhang, Z. Liu, Z. Liu, Int. J. Hydrogen Energy 42 (2017) 7786–7797.
[26] X.-y. Zhao, Y.-p. Xue, C.-f. Yan, Z.-d. Wang, C.-q. Guo, S.-l. Huang, Chem. Eng. Process. Process. Intensif. 119 (2017) 106–112.
[27] J. Fermoso, M.V. Gil, F. Rubiera, D. Chen, ChemSusChem 7 (2014) 3063–3077.
[28] P. Pimenidou, G. Rickett, V. Dupont, M.V. Twigg, Bioresour. Technol. 101 (2010) 9279–9286.
[29] B. Dou, Y. Song, C. Wang, H. Chen, M. Yang, Y. Xu, Appl. Energy 130 (2014) 342–349.
[30] M. Rydén, P. Ramos, Fuel Process. Technol. 96 (2012) 27–36.
[31] B. Dou, H. Zhang, G. Cui, Z. Wang, B. Jiang, K. Wang, H. Chen, Y. Xu, Energy Convers. Manage. 155 (2018) 243–252.
[32] D.P. Harrison, Ind. Eng. Chem. Res. 47 (2008) 6486–6501.
[33] J. Fermoso, L. He, D. Chen, Int. J. Hydrogen Energy 37 (2012) 14047–14054.
[34] A. Lopez Ortiz, D.P. Harrison, Ind. Eng. Chem. Res. 40 (2001) 5102–5109.
[35] K. Johnsen, H.J. Ryu, J.R. Grace, C.J. Lim, Chem. Eng. Sci. 61 (2006) 1195–1202.
[36] D.A. Olivas, M.B. Guerrero, M.E. Bretado, M.M. da Silva Paula, J.S. Gutiérrez, V.G. Velderrain, A.L. Ortiz, V. Collins-Martínez, Int. J. Hydrogen Energy 39 (2014) 16595–16607.
[37] D. Alvarez, J.C. Abanades, Energy Fuels 19 (2005) 270–278.
[38] D. Mess, A.F. Sarofim, J.P. Longwell, Energy Fuels 13 (1999) 999–1005.
[39] V. Manovic, E.J. Anthony, Ind. Eng. Chem. Res. 49 (2010) 6916–6922.
[40] M. Broda, A.M. Kierzkowska, C.R. Müller, Environ. Sci. Technol. 46 (2012) 10849–10856.
[41] T. Noor, M.V. Gil, D. Chen, Appl. Catal. B Environ. 150 (2014) 585–595.

[42] G. Wu, C. Zhang, S. Li, Z. Huang, S. Yan, S. Wang, X. Ma, J. Gong, Energy Environ. Sci. 5 (2012) 8942–8949.
[43] C. Salvador, D. Lu, E.J. Anthony, J. Abanades, Chem. Eng. J. 96 (2003) 187–195.
[44] V. Manovic, E.J. Anthony, Environ. Sci. Technol. 42 (2008) 4170–4174.
[45] L. Li, D.L. King, Z. Nie, X.S. Li, C. Howard, Energy Fuels 24 (2010) 3698–3703.
[46] C.S. Martavaltzi, A.A. Lemonidou, Microporous Mesoporous Mater. 110 (2008) 119–127.
[47] J.A. Moulijn, M. Makkee, A.E. Van Diepen, Chemical Process Technology, John Wiley & Sons, 2013.
[48] W. Liu, H. An, C. Qin, J. Yin, G. Wang, B. Feng, M. Xu, Energy Fuels 26 (2012) 2751–2767.
[49] P. Fennell, J. Davidson, J. Dennis, A. Hayhurst, J. Energy Inst. 80 (2007) 116–119.
[50] V. Manovic, E.J. Anthony, Environ. Sci. Technol. 41 (2007) 1420–1425.
[51] V. Materić, S. Edwards, S.I. Smedley, R. Holt, Ind. Eng. Chem. Res. 49 (2010) 12429–12434.
[52] J. Blamey, D.Y. Lu, P.S. Fennell, E. Anthony, Ind. Eng. Chem. Res. 50 (2011) 10329–10334.
[53] J. Blamey, V. Manovic, E.J. Anthony, D.R. Dugwell, P.S. Fennell, Fuel 150 (2015) 269–277.
[54] O.A. Omoniyi, V. Dupont, Appl. Catal. B Environ. 226 (2018) 258–268.
[55] J. Blamey, E. Anthony, J. Wang, P. Fennell, Prog. Energy Combust. Sci. 36 (2010) 260–279.
[56] K. Tzanetis, C. Martavaltzi, A. Lemonidou, Int. J. Hydrogen Energy 37 (2012) 16308–16320.
[57] R.M. Zin, Advanced Steam Reforming of Pyrolysis Oils and Their Aqueous Phase, School of Process, Environmental and Materials Engineering, University of Leeds, Energy and Research Institute, 2012.
[58] F. Cheng, V. Dupont, Int. J. Hydrogen Energy 38 (2013) 15160–15172.
[59] S. Gordon, B.J. McBride, Computer Program for Calculation of Complex Chemical Equilibrium Compositions and Applications, National Aeronautics and Space Administration, Office of Management, Scientific and Technical Information Program, 1996.
[60] P. Pimenidou, Novel Process of Hydrogen Production From Liquids of Biomass Origin, School of Process, Environmmental and Material Engineering, University of Leeds, 2010.
[61] S. Bhatia, D. Perlmutter, AIChE J. 29 (1983) 79–86.
[62] P. Sun, J.R. Grace, C.J. Lim, E.J. Anthony, Chem. Eng. Sci. 63 (2008) 57–70.
[63] H. Gupta, L.-S. Fan, Ind. Eng. Chem. Res. 41 (2002) 4035–4042.
[64] J.C. Abanades, D. Alvarez, Energy Fuels 17 (2003) 308–315.
[65] A. Lysikov, A. Okunev, O. Netskina, Int. J. Hydrogen Energy 38 (2013) 10354–10363.
[66] F. Cheng, V. Dupont, M.V. Twigg, Appl. Catal. B Environ. 200 (2017) 121–132.
[67] F. Cheng, V. Dupont, M.V. Twigg, Appl. Catal. A Gen. 527 (2016) 1–8.